

# A study of $\bar{p}p \rightarrow \eta\eta\eta$ for masses 1960 to 2410 MeV/c<sup>2</sup>

A.V. Anisovich<sup>c</sup>, C.A. Baker<sup>a</sup>, C.J. Batty<sup>a</sup>, D.V. Bugg<sup>b</sup>, V.A. Nikonov<sup>c</sup>, A.V. Sarantsev<sup>c</sup>, V.V. Sarantsev<sup>c</sup>, B.S. Zou<sup>b 1</sup>

<sup>a</sup> Queen Mary and Westfield College, London E14NS, UK

<sup>b</sup> Rutherford Appleton Laboratory, Chilton, Didcot OX11 0QX, UK

<sup>c</sup> PNPI, Gatchina, St. Petersburg district, 188350, Russia

## Abstract

Data on  $\bar{p}p \rightarrow \eta\eta\eta$  for beam momenta 600–1940 MeV/c are presented. The strongest channel is  $f_0(1500)\eta$  from the initial  $\bar{p}p$  state  $^1S_0$ . Together with  $\eta\pi^0\pi^0$  data, the  $3\eta$  data determine the branching ratio  $BR[f_0(1500) \rightarrow \eta\eta]/BR[f_0(1500) \rightarrow \pi^0\pi^0] = 0.42 \pm 0.09$ . They are consistent with a dominant contribution from an  $I = 0, C = +1, J^{PC} = 0^{-+}$  resonance observed earlier in the  $\eta\pi^0\pi^0$  data; from the combined  $\eta\pi^0\pi^0$  and  $\eta\eta\eta$  data, its mass is  $M = 2320 \pm 15$  MeV and its width  $\Gamma = 230 \pm 35$  MeV.

As part of a study of  $\bar{p}p$  annihilation in flight to neutral final states, we have earlier presented results on  $\bar{p}p \rightarrow \eta\pi^0\pi^0$  [1], with statistics of typically 70,000 events per momentum. We have at the same time collected statistics of up to 192 events per momentum on  $\bar{p}p \rightarrow \eta\eta\eta$  in the  $6\gamma$  channel. Despite the limited statistics, some useful conclusions may be drawn.

In  $\eta\pi^0\pi^0$  data, the  $f_2(1270)\eta$  final state is dominant; the contribution from  $f_0(1500)\pi$  is small at all beam momenta: up to 3.2% with errors of  $\sim 0.6\%$  at each momentum. However, the branching ratio of  $f_0(1500)$  to  $\eta\eta$  is a factor  $\sim 45$  larger than for  $f_2(1270)$ ; consequently  $f_0(1500)$  makes the larger contribution to  $3\eta$  data. These data therefore provide a valuable check on some features of the most recent amplitude analysis of  $\bar{p}p \rightarrow \eta\pi^0\pi^0$ ; this has recently been analysed in a combined fit with data on  $\bar{p}p \rightarrow \pi^0\pi^0, \eta\eta, \eta\eta'$  and  $\pi^-\pi^+$  [2]. A  $0^-$  resonance found at  $\sim 2285$  MeV in that analysis is predicted to be the main feature of the  $f_0(1500)\eta$  channel here. The present  $3\eta$  data allow an improvement in the determination of its mass and width.

The data were taken at LEAR using the Crystal Barrel detector. Experimental details have been given in Ref. [1], and here we consider only features which involve identification of the  $3\eta$  final state. In order to isolate this rare channel in  $6\gamma$  data, tight selection criteria are needed to eliminate backgrounds from other channels. In processing data, we first demand exactly six photon showers, each confined to a block of  $3 \times 3$  adjacent CsI crystals of the detector. Extra energy deposits produced by Compton scattering out of the primary showers into nearby crystals (so-called 'split-offs') appear in  $\sim 50\%$  of events. All attempts to recover such events lead to backgrounds higher by typically a factor 3–6. We therefore reject events containing such additional energy deposits. Events where two photons from one  $\pi^0$  merge into a single shower are also discarded.

A least squares kinematic fit is first required to  $\bar{p}p \rightarrow 6\gamma$ , satisfying energy-momentum conservation with confidence level  $CL > 10\%$ . Then 7C fits are made to all 3-particle final states involving  $\pi^0, \eta$  or  $\eta'$ . We reject events which fit  $3\pi^0, \eta\pi^0\pi^0, \eta\eta\pi^0, \eta'\pi^0\pi^0$  or  $\eta\eta'\pi^0$  with  $CL > 10^{-4}$ . As further rejection against the prolific  $3\pi^0, \eta\pi^0\pi^0$  and  $\eta\eta\pi^0$  channels, events are rejected if they fit  $\pi^0\pi^0\gamma\gamma$  or  $\pi^0\eta\gamma\gamma$  with  $CL > 10^{-4}$ .

---

<sup>1</sup>Now at IHEP, Beijing 100039, China

Channel	Background (%)
$\eta\eta\pi^0$	0.1
$\eta\pi^0\pi^0\pi^0$	0.1
$\eta\eta\pi^0\pi^0$	1.1
$\omega\eta\eta, \omega \rightarrow \pi^0\gamma$	0.9
$\omega\eta\pi^0, \omega \rightarrow \pi^0\gamma$	0.1

Table 1: Background levels in  $6\gamma$  data from competing channels at 1800 MeV/c.

A Monte Carlo study using 20,000 generated events for all competing channels shows that the main sources of potential background are  $\eta\eta\pi^0$ ,  $\eta\pi^0\pi^0\pi^0$ ,  $\eta\eta\pi^0\pi^0$ , and  $\omega\eta\pi^0$  or  $\omega\eta\eta$  where  $\omega \rightarrow \pi^0\gamma$ . In the last four cases, two photons or one go undetected. The background levels at 1800 MeV/c from competing channels are estimated from this Monte Carlo simulation and are summarised in Table 1. The principal backgrounds arise from  $\omega\eta\eta$  and  $\eta\eta\pi^0\pi^0$ . The situation is similar at other momenta and the total surviving background is 2.3% within errors at all momenta. Kinematic fits to the  $\eta\eta\gamma\gamma$  hypothesis are consistent with this estimate and show only a few scattered events with  $M(\gamma\gamma)$  outside the  $\eta \rightarrow \gamma\gamma$  peak.

Momentum (MeV/c)	$3\eta$ events	$\epsilon$	$\sigma(3\eta)$ ( $\mu b$ )
600	9	0.130	$3.0 \pm 0.7$
900	68	0.126	$4.3 \pm 0.4$
1050	72	0.126	$5.0 \pm 0.5$
1200	157	0.124	$6.9 \pm 0.5$
1350	103	0.121	$6.4 \pm 0.5$
1525	99	0.117	$8.3 \pm 0.6$
1642	142	0.115	$9.8 \pm 0.6$
1800	192	0.113	$9.5 \pm 0.5$
1940	163	0.112	$5.7 \pm 0.4$

Table 2: Numbers of  $3\eta$  events after background subtraction and reconstruction efficiency  $\epsilon$ ; the last column shows the weighted mean of the integrated cross section for  $3\eta$  (corrected for all  $\eta$  decays) from  $6\gamma$  and  $10\gamma$  data. Errors include statistics and the uncertainty in normalisation of cross sections at individual momenta from Ref. [3]

Columns 2 and 3 of Table 2 show the number of surviving  $3\eta$  events and also the reconstruction efficiency  $\epsilon$ . This efficiency is estimated by generating  $\geq 50,000$  Monte Carlo events at every momentum. These events are subjected to identical selection procedures to data and are used for the maximum likelihood fit described below. Cross sections are derived from the number of observed events, corrected by the efficiencies of Table 2 and using the number of incident antiprotons and the target length of 4.4 cm. A correction is applied for an observed dependence of reconstruction efficiency as a function of beam rate; this is described in full in Ref. [3].

As a check, the  $10\gamma$  data have also been examined for the final state  $\eta\eta 3\pi^0$ , where one  $\eta \rightarrow 3\pi^0$ . Events are selected by demanding exactly 10 photon showers and a kinematic fit to

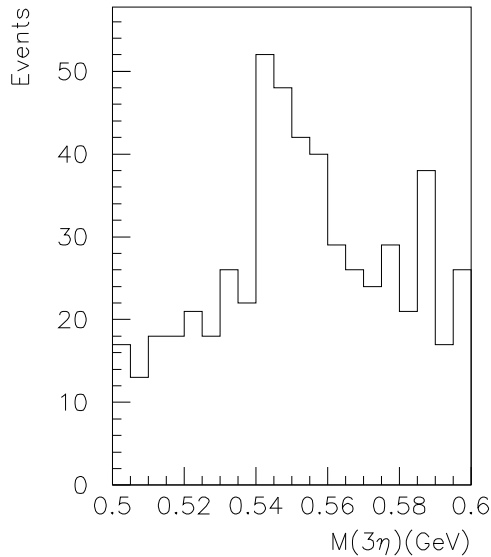


Figure 1: The  $\eta \rightarrow 3\pi^0$  peak in  $\bar{p}p \rightarrow \eta\eta 3\pi^0$  data at 900 MeV/c.

$\eta\eta 3\pi^0$  with  $CL > 10\%$ . Events fitting  $5\pi^0$  or  $\eta 4\pi^0$  with  $CL > 0.1\%$  are rejected. Unfortunately, the background level under the  $\eta \rightarrow 3\pi^0$  peak is substantial (20% of the signal at the highest momenta, rising to 80% at the lowest). It arises mostly from  $\eta\eta 3\pi^0$  and cannot be reduced. It is illustrated at 900 MeV/c in Fig. 1. This background level is too high to allow a physics analysis. However, these events may be used, after subtracting background, to check the evaluation of integrated cross sections. Fig. 2 compares cross sections for  $\bar{p}p \rightarrow 3\eta$  from  $6\gamma$  events (circles joined by the full curve) and  $10\gamma$  events (squares joined by the dashed curve). There is agreement between these two determinations within the errors. The last column of Table 2 shows the weighted mean of the integrated cross sections from  $6\gamma$  and  $10\gamma$  data. A detail is that statistics at 600 MeV/c are much lower than at other momenta; this accounts for the small number of events, despite a similar cross section to that at 900 MeV/c.

Dalitz plots from  $6\gamma$  data and projections on to  $M(\eta\eta)$  are shown at 8 beam momenta from 1940 to 900 MeV/c in Figs. 3 and 4. Processes which need to be considered are:

$$\bar{p}p \rightarrow f_0(1500)\eta \quad (1)$$

$$\rightarrow \sigma\eta \quad (2)$$

$$\rightarrow f_2(1270)\eta \quad (3)$$

$$\rightarrow f_0(1370)\eta \quad (4)$$

$$\rightarrow f_2'(1525)\eta \quad (5)$$

Of these, the last two turn out to be negligible. The  $f_0(1500)$  is conspicuous at the higher momenta. The  $f_2(1270)$  is obscured in mass projections of Figs. 3 and 4 by reflections from the stronger  $f_0(1500)$ . The fit shows that it makes a small but significant contribution. The  $\sigma\eta$  channel makes a strong contribution to  $\eta\pi^0\pi^0$  data, so its presence in  $3\eta$  is necessary; it accounts well for the small uniform component over the Dalitz plots of Figs. 3 and 4. Here  $\sigma$  is

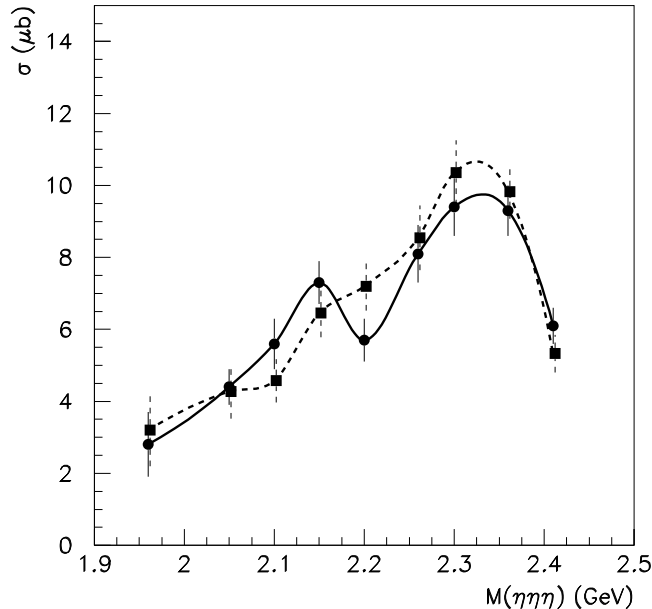


Figure 2: Comparison of integrated cross sections from  $6\gamma$  data (circles and full curve) with that from  $10\gamma$  data (triangles and dashed curve).

a shorthand for the  $f_0(400 - 1200)$  of the Particle Data Group (PDG) [4]. It is fitted with the parametrisation of Zou and Bugg [5].

The data have been fitted by the maximum likelihood method. Present data are closely related to those for  $\bar{p}p \rightarrow \eta\pi^0\pi^0$ , where statistics are much higher. Our strategy is to take magnitudes and phases of all partial waves for  $f_2(1270)\eta$ ,  $f_0(1500)\eta$  and  $\sigma\eta$  from our analysis of  $\eta\pi^0\pi^0$  [2], allowing one free parameter to determine the branching ratio  $r_{1270} = BR[f_2(1270) \rightarrow \eta\eta]/BR[f_2(1270) \rightarrow \pi^0\pi^0]$ , a second to determine the branching ratio  $r_{1500} = BR[f_0(1500) \rightarrow \eta\eta]/BR[f_0(1500) \rightarrow \pi^0\pi^0]$  and a third to determine the branching ratio  $r_\sigma = BR[\sigma \rightarrow \eta\eta]/BR[\sigma \rightarrow \pi^0\pi^0]$ . The contribution from  $f_2(1270)$  is small, as shown below in Fig. 6(b) by the chain curve. The value of  $r_{1270}$  can therefore be set to the PDG value. The absolute value of the integrated cross section for  $3\eta$  is sensitive to  $r_{1500}$  and  $r_\sigma$ , where therefore need to be fitted.

Momentum	$-f_0(1500)\eta$	$-f_2(1270)\eta$	$+f_0(1370)\eta$	$+f_2'(1525)\eta$
900	-27.6	-4.4	1.1	1.2
1050	-25.9	-10.8	1.8	0.9
1200	-44.9	-1.0	1.0	0.1
1350	-56.6	-7.1	2.2	0.8
1525	-15.0	-19.8	0.8	1.7
1642	-21.8	-41.6	4.4	2.0
1800	-95.2	-20.6	0.3	0.5
1942	-50.6	-11.5	4.8	1.1

Table 3: Changes in log likelihood (a) removing  $f_0(1500)\eta$  from the fit, (b) removing  $f_2(1270)\eta$ , (c) adding  $f_0(1370)\eta$  and (d) adding  $f_2'(1525)\eta$ .

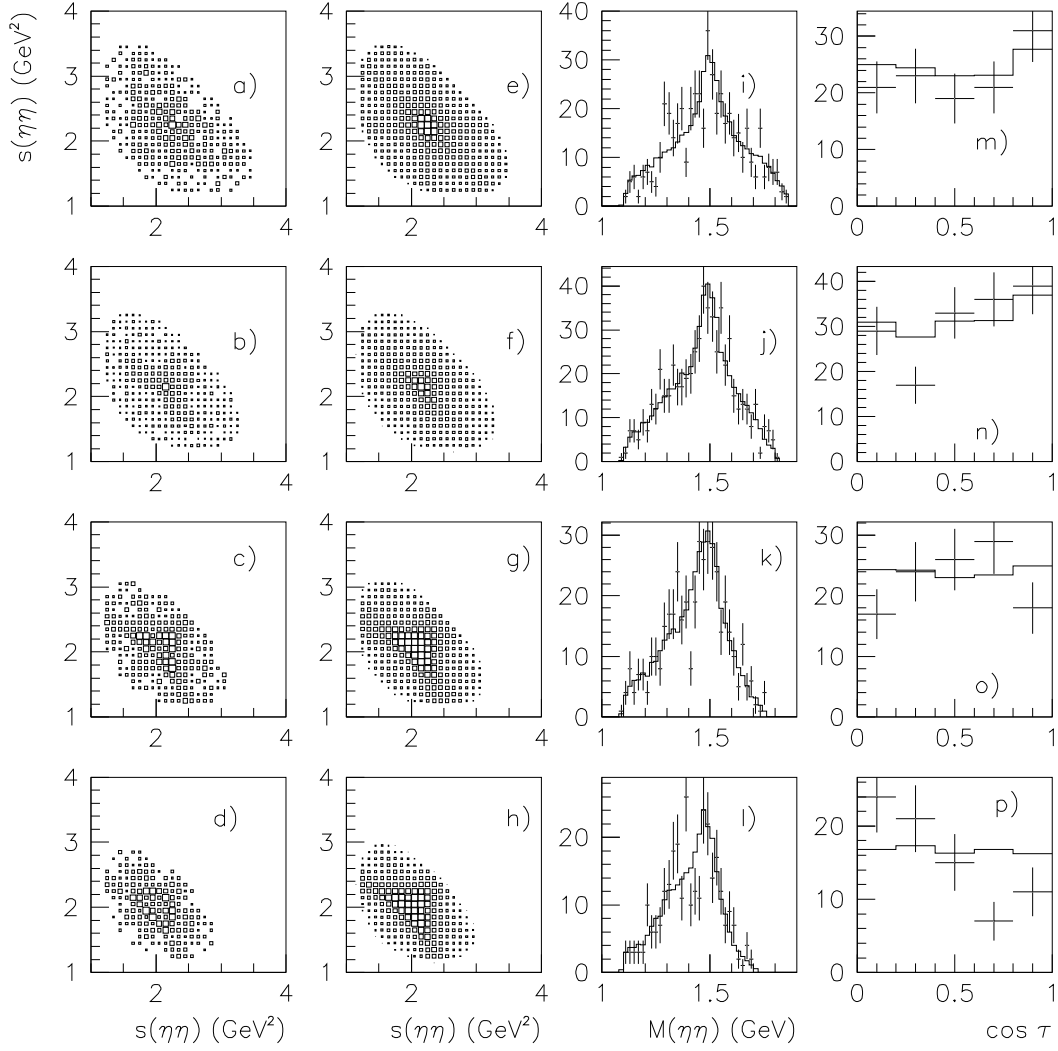


Figure 3: (a)–(d) Dalitz plots of data at beam momenta of 1940, 1800, 1642 and 1525 MeV/c, (e)–(h) fitted Dalitz plots, (i)–(l) projections on to  $M(\eta\eta)$ , (m)–(p) production angular distribution for events in a band 120 MeV wide centred on  $f_0(1500)$ . Histograms show the fit.

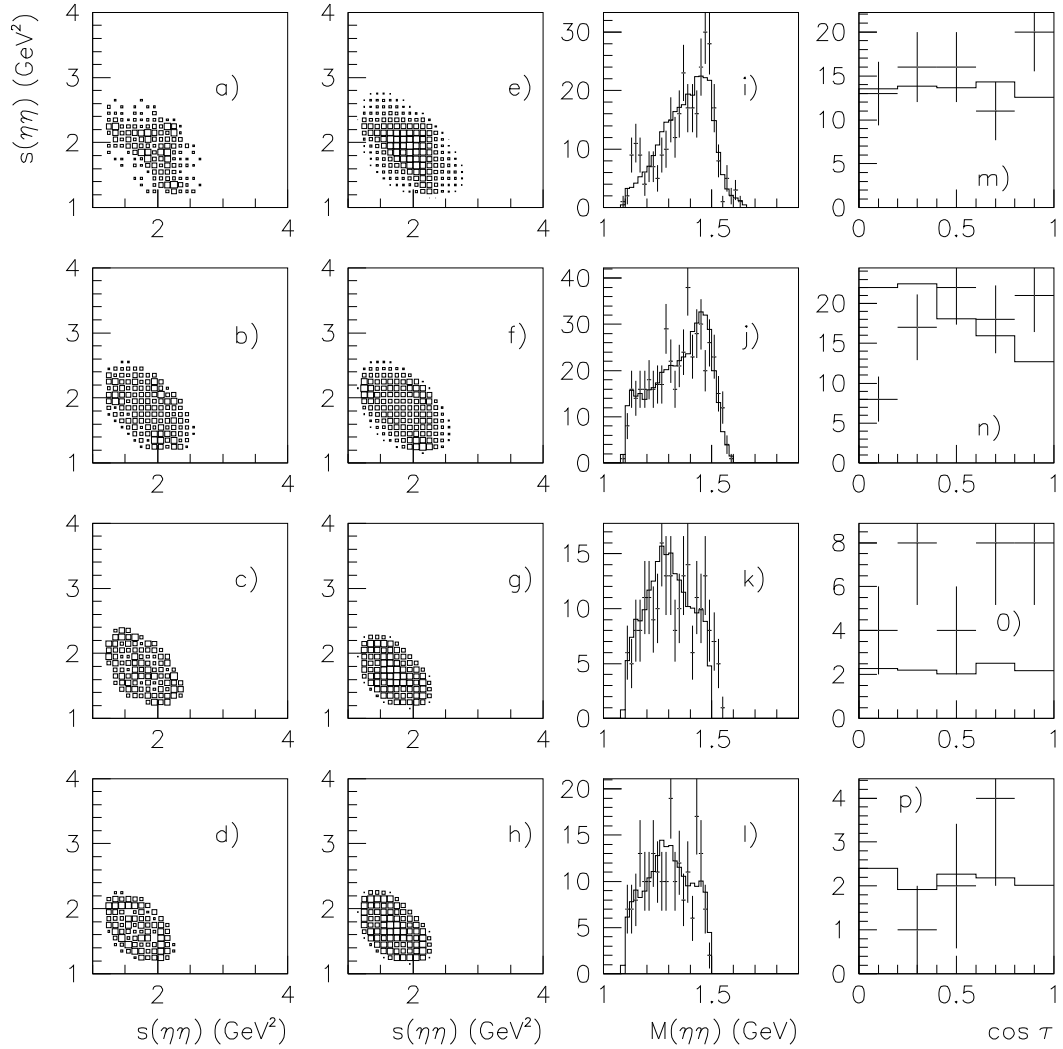


Figure 4: As Fig. 1 at 1350, 1200, 1050 and 900 MeV/c.

Columns 2 and 3 of Table 3 show changes in log likelihood when  $f_0(1500)$  or  $f_2(1270)$  is removed from the fit at individual momenta. Our definition is such that a change of log likelihood of 0.5 corresponds to a one standard deviation change for one degree of freedom, so the observed changes indicate the presence of both channels. Dropping  $f_2(1270)$  from the overall fit to all momenta, log likelihood is worse by 90.4.

Histograms on Figs. 3 and 4 display results of the fit to all momenta simultaneously. The first column of Dalitz plots shows data and the second column the fits. Every event is plotted in three  $\eta\eta$  combinations. The low statistics cause substantial fluctuations for data and are responsible for some apparent disagreement with the fit; the latter is much smoother than data since Monte Carlo statistics of over 5000 events per momentum are used in the maximum likelihood fit. In fact, the  $\chi^2$  between data and fit on the Dalitz plot averages 1.1 per point, so there is no discrepancy.

The partial wave amplitude for production of the  $f_2$  between particles 1 and 2 will be used as an illustration of the way amplitudes are parametrised. It takes the form

$$f = \frac{G}{M^2 - s_{12} - iM\Gamma} B_2(k) B_L(p) Z(p, k). \quad (6)$$

Here  $G$  is a complex coupling constant, the denominator refers to the  $f_2(1270)$ ,  $s$  is mass squared for the  $\eta_1\eta_2$  combination, and  $Z$  is a relativistic Zemach tensor given explicitly in Ref. [1]. The cross section is obtained from the coherent sum of amplitudes for the three  $\eta\eta$  combinations. The value of  $G$  for  $3\eta$  data is related to that for  $\eta\pi^0\pi^0$  by  $G(3\eta) = \sqrt{r_{1270}k_\pi/k_\eta} G(\eta\pi^0\pi^0)/\sqrt{3}$ . The factor  $1/\sqrt{3}$  allows for the three identical  $\eta\eta$  pairs; the ratio  $\sqrt{k_\pi/k_\eta}$ , involving momenta  $k$  of  $\pi$  and  $\eta$  in the decay  $f_2 \rightarrow \pi\pi$  and  $\eta\eta$ , allows for phase space for those decays. Standard Blatt-Weisskopf centrifugal barrier factors  $B_L$  with radius 0.8 fm are used to parametrise the dependence on the centre of mass momentum  $p$  with which the resonance is produced, with orbital angular momentum  $L$ , and also on its decay momentum  $k$  in the resonance rest frame.

The complex coupling constant  $G$  assigns a phase to each partial wave. This phase originates from the initial state  $\bar{p}p$  interaction and from rescattering in the final state. The approximation we adopt is that the phase is the same for decays  $f_2(1270) \rightarrow \eta\eta$  and  $f_2(1270) \rightarrow \pi^0\pi^0$  and likewise for  $f_0(1500) \rightarrow \eta\eta$  and  $\pi^0\pi^0$ . This is in the spirit of the isobar model, where it is assumed that the final resonant state is reached after any number of intermediate rescatterings and then decays into the  $\eta\eta$  and  $\pi^0\pi^0$  channels with the same phase. Relative magnitudes of  $f_2(1270)$  contributions in different partial waves are taken from the fit to  $\eta\pi^0\pi^0$  data of Ref. [2]; likewise for  $f_0(1500)$  and  $\sigma$  contributions. However, rescattering is possible in  $\eta\pi^0\pi^0$  to additional final states  $a_2(1320)\pi^0$  and  $a_0(980)\pi^0$ ; therefore we allow an overall phase difference of  $f_2(1270)\eta$  relative to  $f_0(1500)\eta$  and  $\sigma\eta$  at all momenta between  $\eta\pi^0\pi^0$  data and  $3\eta$ . The fit to  $3\eta$  is therefore related to that to  $\eta\pi^0\pi^0$  by 4 parameters: two relative phases between  $f_2(1270)\eta$ ,  $f_0(1500)\eta$  and  $\sigma\eta$  and two branching ratios  $r_{1500}$  and  $r_\sigma$ , common to all momenta. Because the contribution from  $f_2(1270)$  is small, results concerning  $f_0(1500)\eta$  have little sensitivity to the detailed partial wave decomposition of  $f_2(1270)\eta$ . This is because correlations between the two channels arise only where bands cross on the Dalitz plots and involve rather few events.

The prediction from  $\eta\pi^0\pi^0$  data [2] is that the dominant contribution to  $3\eta$  will be from  $L = 0$  decays of a  $0^-$  resonance at 2285 MeV. A small  $L = 2$  component is predicted, roughly 15% of the intensity of  $L = 0$ . Contributions with  $L = 1$  and 3 are found in Ref. [2] to be very small.

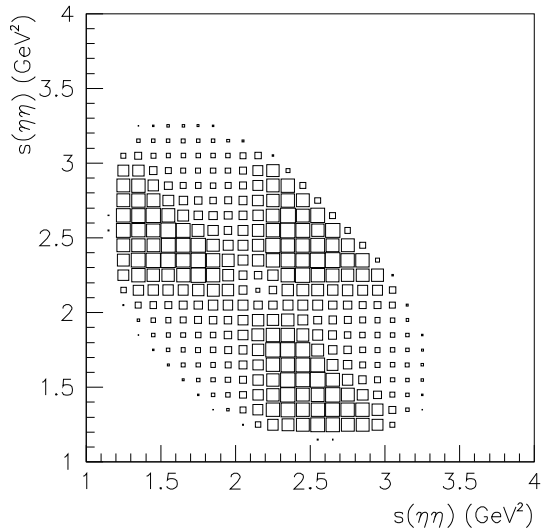


Figure 5: The predicted Dalitz plot at 1800 MeV/c for  ${}^3P_1 \rightarrow f_0(1500)\eta$ .

For  $f_0(1500)\eta$  final states, the angular distributions against centre of mass production angle  $\tau$  are shown in Figs. 3 and 4. Fortuitously, the  $L = 0$  and  $L = 2$  amplitudes are nearly orthogonal, with the result that interferences between them are small. Hence angular distributions in Fig. 3 and 4 are close to isotropic. The discrepancy between data and fit in Figs. 4(o) is associated with the very small number of events in the  $f_0(1500)$  mass region.

A point with interesting consequences is that the three  $f_0(1500)$  bands cross at the centre of the Dalitz plot near a beam momentum of 1800 MeV/c. The strong constructive interference observed in Fig. 3(b) between the three bands requires that the process goes largely through a single  $\bar{p}p$  partial wave with even  $L$ . Amplitudes for production with  $L = 1$  cancel at the intersection point of the three bands and their sum changes sign about this point. To see this, consider  $f_0(1500)$  production from the initial state  ${}^3P_1$ . For initial helicity  $m = 0$ , the Clebsch-Gordan coefficient for coupling to  $\bar{p}p$  is zero. For  $m = 1$ , the amplitude is proportional to  $p \sin \tau \exp(i\phi)$ , where  $\tau$  is the polar angle for production of the resonance and  $\phi$  is the associated azimuthal angle. This amplitude is therefore proportional to  $p_X + ip_Y$ , where  $p_{X,Y}$  are transverse momentum components of the resonance. For the coherent superposition of the three  $f_0(1500)\eta$  combinations, the resultant at the intersection of the three bands is zero, by momentum conservation. The same result extends to  $L = 3$  for  $f_0(1500)\eta$  and to production of  $f'_2(1525)$  with  $L = 1$  and 3, though the amplitude then contains additional factors for the  $f'_2$  decay. Fig. 5 shows the predicted Dalitz plot for  ${}^3P_1 \rightarrow f_0(1500)\eta$  at 1800 MeV/c. This distinctive pattern is absent from the data of Fig. 3. The amplitude analysis confirms that any  $L = 1$  or 3 processes producing  $f_0(1500)$  or  $f'_2(1525)$  at 1642, 1800 and 1940 MeV/c are absent or very weak (summed cross sections  $\leq 10\%$  of  $L = 0$ ).

The essential physics conclusions of the amplitude analysis are illustrated in Fig. 6. Fig. 6(a) shows a fit (with details given below) to the integrated  $3\eta$  cross section averaged between  $6\gamma$  and  $10\gamma$  data. The peak requires, as predicted, a dominant contribution from a  $J^P = 0^-$  resonance in the  $f_0(1500)\eta$  channel; its intensity is shown by the full curve in Fig. 6(b). It appears at a slightly higher mass than predicted:  $2328 \pm 16$  MeV compared with  $M = 2285 \pm 20$  MeV of Ref. [2]. The shift is compatible with the combined errors of the two analyses. The width is



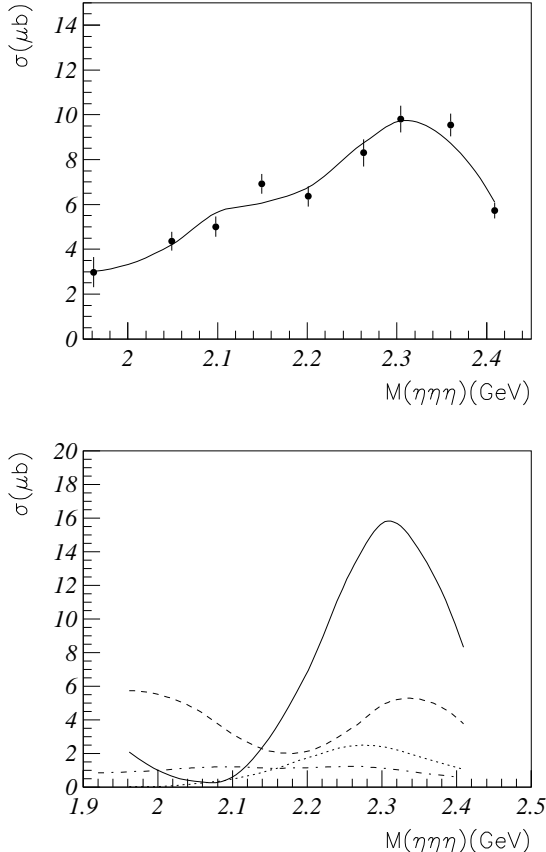


Figure 6: (a) The fit to the mean integrated cross section from  $6\gamma$  and  $10\gamma$  data; (b) the contributions from  $\eta(2320) \rightarrow [f_0(1500)\eta]_{L=0}$  (full curve),  $\sigma\eta$  (dashed),  $\eta_2(2267) \rightarrow [f_0(1500)\eta]_{L=2}$  (dotted), and  $f_2(1270)\eta$  (chain curve).

discussed below.

In addition, a  $\sigma\eta$  contribution is required, as shown by the dashed curve. This interferes destructively with  $[f_0(1500)\eta]_{L=0}$ . Thirdly, there is a small contribution, shown dotted, from  $\eta_2(2267) \rightarrow [f_0(1500)\eta]_{L=2}$ . The  $f_2(1270)\eta$  channel makes a small contribution  $< 1.3\mu\text{b}$  for all masses (chain curve).

The  $f_2\eta$  contribution contains too many partial waves and is too small to allow a useful determination of the branching ratio  $r_{1270}$  between  $\eta\eta$  and  $\pi^0\pi^0$ . This parameter is therefore fixed at the PDG value,  $1.35 \times 10^{-2}$  [4]. The corresponding ratio  $r_{1500}$  for  $f_0(1500)$  may be fitted over a range of values, because of interference of this channel with  $\sigma\eta$ . The width of the  $0^-$  resonance at 2330 MeV correlates strongly with  $r_{1500}$ . Small  $r$  values require a narrow width for the resonance, so as to reproduce the peak cross section. Amsler et al. [6] determine from  $\bar{p}p \rightarrow \eta\eta\pi^0$  and  $3\pi^0$  data at rest a ratio  $r_{1500} = 0.47 \pm 0.21$ ; using this value, the width of the  $0^-$  resonance optimises at  $\Gamma = 240$  MeV, distinctly smaller than the value  $325 \pm 30$  MeV found from  $\eta\pi^0\pi^0$  data [2]. The WA102 collaboration [9] finds  $r_{1500} = 0.54 \pm 0.09$ , compatible with Ref. [6] and with our determination below. Abele et al. [6] find  $r_{1500} = 0.23 \pm 0.04$ , which requires  $\Gamma = 154$  MeV for the  $0^-$  resonance. This narrow width gives a significantly poorer log likelihood in fitting  $3\eta$  data and is hard to reconcile with  $\eta\pi^0\pi^0$  data.

We find that the fit to  $\eta\pi^0\pi^0$  data will adjust towards these new values of  $M$  and  $\Gamma$  with only a minor change in log likelihood and in other partial waves. The optimum fit to combined  $3\eta$  and  $\eta\pi^0\pi^0$  data gives  $M = 2320 \pm 15$  MeV,  $\Gamma = 230 \pm 35$  MeV and

$$r_{1500} = 0.39 \pm 0.09. \quad (7)$$

These values are used in the curves of Fig. 6. Intensities derived from each component are shown in Fig. 6(b) including interferences between all three  $\eta\eta$  channels and after integrating over the Dalitz plot. In comparing with corresponding intensities for the  $\eta\pi\pi$  channel, shown in Fig. 2 of Ref. [2], one must take note of two points. Firstly, strong constructive interferences between the three  $\eta\eta$  channels in  $3\eta$  enhance the peaks of Fig. 6(b), for example by 60% for  $[f_0(1500)\eta]_{L=0}$ . Secondly, Fig. 6(b) uses a width of 230 MeV for the resonance, while Fig. 2 of Ref. [3] uses 325 MeV; this increases the peak height in Fig. 6(b) by a further factor 1.9.

The  $\sigma\eta$  intensity in Fig. 6(b) is  $\sim 20\%$  of that for  $\eta\pi^0\pi^0$ . If the  $\sigma$  is dominantly non-strange, one expects from the composition of the  $\eta$ , namely

$$|\eta\rangle = 0.8|(u\bar{u} + d\bar{d})/\sqrt{2}\rangle - 0.6|s\bar{s}\rangle,$$

a ratio between  $\eta\eta$  and  $\pi^0\pi^0$  decay of  $(0.8)^4 < k_\eta/k_\pi >$ ; here  $k_{\eta,\pi}$  are the momenta in the  $\sigma$  rest frame in  $\eta\eta$  and  $\pi\pi$  decays respectively. Averaging over phase space for the  $\sigma$ , one finds  $< k_\eta/k_\pi > \simeq 0.6$ , and hence a predicted intensity for  $\sigma\eta$  in  $3\eta$  of 25% of that in  $\eta\pi^0\pi^0$ , close to the fit.

From present data, we are unable to demonstrate the presence of the  $J^P = 2^-$  resonance decaying to  $[f_0(1500)\eta]_{L=2}$ . Deviations from isotropy in angular distributions of Figs. 3 and 4 are too small to demonstrate its presence, though angular distributions are compatible with prediction within the large errors. We remark that the  $2^-$  resonance is observed clearly in data on  $\bar{p}p \rightarrow \eta'\pi^0\pi^0$ , where it makes a dominant contribution in decays to  $f_2(1270)\eta'$  [9].

The fourth and fifth columns of Table 3 show changes in log likelihood when either  $f_0(1370)\eta$  or  $f'_2(1525)$  is added to the fit with  $L = 0$ . Statistically one expects an improvement of 1 for two extra fitted parameters. The evidence for either  $f_0(1370)$  or  $f'_2(1525)$  being present is insignificant. Let  $\alpha$  be the decay angle with respect to the beam in the rest frame of the resonance. The decay angular distribution  $(3\cos^2\alpha - 1)$  for  $f'_2(1525)$  produced from the initial state  $^1D_2$  with  $L = 0$  is distinctive and the amplitude would interfere with  $f_0(1500)\eta$ . The  $L = 1$  production amplitude likewise gives a distinctive contribution to the Dalitz plot, similar to that of Fig. 5. The mean fitted value of its cross section is 15% of  $f_0(1500)\eta$  but some or all of this is undoubtedly statistical noise in the fit.

From earlier analysis of  $\bar{p}p \rightarrow \eta\eta\pi^0$  and  $3\pi^0$  at rest, the ratio  $BR[f_0(1370) \rightarrow \eta\eta]/BR[f_0(1370) \rightarrow \pi^0\pi^0] = 0.056 \pm 0.04$  [6]. Despite the sizeable error, there was no doubt of the presence of some  $f_0(1370) \rightarrow \eta\eta$  signal in the  $\eta\eta\pi^0$  data [7], considerably higher than that for  $f_2(1270)$ . From the small  $f_0(1370)\eta$  signal in  $3\eta$ , we therefore deduce that the signal observed in  $\eta\pi^0\pi^0$  must be almost entirely  $f_2(1270)\eta$  with very little  $f_0(1370)\eta$ . This is a useful check on the analysis of  $\eta\pi^0\pi^0$ , where a small  $f_0(1370)$  signal is hard to identify in the presence of a dominant  $f_2(1270)\eta$  contribution.

In summary, despite low statistics, four results emerge from this analysis.

- The  $3\eta$  and  $\eta\pi^0\pi^0$  data together require an  $I = 0$ ,  $C = +1$ ,  $J^{PC} = 0^{-+}$  resonance with  $M = 2320 \pm 10$  MeV,  $\Gamma = 230 \pm 35$  MeV, decaying to  $f_0(1500)\eta$ .

- The ratio of intensities in  $3\eta$  and  $\eta\pi^0\pi^0$  gives  $r_{1500} = 0.39 \pm 0.09$ .
- The ratio of  $\sigma\eta$  intensities in  $3\eta$  and  $\eta\pi^0\pi^0$  is close to that expected for non-strange composition of  $\sigma \equiv f_0(400 - 1200)$ .
- The absence of  $f_0(1370) \rightarrow \eta\eta$  in  $3\eta$  data is a useful check that it makes very little contribution to  $\eta\pi^0\pi^0$  data.

We wish to thank the technical staff of the LEAR machine group and of all the participating institutions for their invaluable contributions to the success of the experiment. We thank the Crystal Barrel group for allowing use of the data. We acknowledge financial support from the British Particle Physics and Astronomy Research Council (PPARC). The St. Petersburg group wishes to acknowledge financial support from PPARC and INTAS grant RFBR 95-0267.

## References

- [1] A.V. Anisovich et al, Phys. Lett. B452 (1999) 173; Nucl. Phys A651 (1999) 253.
- [2] A.V. Anisovich et al., *I = 0 C = +1 mesons from 1920 to 2410 MeV/c<sup>2</sup>*, Phys. Lett. B (in press).
- [3] A.V. Anisovich et al., Phys. Lett. B468 (1999) 304; Nucl. Phys. A662 (2000) 344.
- [4] Particle Data Group, Euro. Phys. J. C3 (2000) 1.
- [5] B.S. Zou, D.V. Bugg, Phys. Rev. D48 (1993) R3948.
- [6] C. Amsler et al., Phys. Lett. B355 (1995) 425.
- [7] D. Barberis et al., Phys. Lett. B479 (2000) 59.
- [8] A. Abele et al., Nucl. Phys. A609 (1996) 562.
- [9] A.V. Anisovich et al., *Data on  $\bar{p}p \rightarrow \eta'\pi^0\pi^0$  for masses 1960 to 2410 MeV/c<sup>2</sup>*, Phys. Lett. B (in press).
- [10] C. Amsler et al., Phys. Lett. B353 (1995) 571.